Compositional relaxation on the approach to the glass transition in a model trehalose solution

Stephen D. W. Hannam, Peter J. Daivis,* and Gary Bryant
School of Science and Centre for Molecular and Nanoscale Physics, RMIT University, GPO Box 2476, Melbourne Victoria 3001, Australia

(Received 23 November 2018; published 7 March 2019)

Molecular dynamics simulation was used to study the temperature dependence of the mutual diffusion coefficient D_m and the intermediate scattering function of equilibrium and metastable aqueous solutions of the cryoprotectant molecule trehalose at very low (2.2 and 9 wt.%) and very high (80 and 95 wt.%) concentrations. The simulations were conducted over a range of temperatures approaching the glass transition temperature T_g for each concentration. Similar to a recent observation made on a glass-forming model polydisperse colloidal suspension [Hannam *et al.*, Phys. Rev. E **96**, 022609 (2017)], we confirmed by a set of independent computations that D_m is responsible for the long-time decay of the intermediate scattering function. We observed that D_m decreased on the approach to the glass transition temperature, resulting in an extremely slow long-time decay in the intermediate scattering function that culminated in the arrest of compositional fluctuations and a plateau in the intermediate scattering function at T_g. In both cases, crystallization requires a change in the composition of the solution, which is a process controlled by D_m. This transport coefficient can either increase or decrease as solidification is approached, because it depends on a product of thermodynamic and mobility factors. Our observations show that in both cases, for the glass-forming liquids, it is observed to decrease, while for a previously studied monodisperse colloidal suspension which crystallizes easily, it increases. The similarity in the behavior of these two very different glass-forming systems (the polydisperse colloidal suspension and the sugar solution) shows the importance of the mutual diffusion coefficient to our understanding of vitrification and suggests a possible distinction between between glass-forming and crystallizing solutions.

DOI: 10.1103/PhysRevE.99.032602

I. INTRODUCTION

The cryopreservation of biological cells and tissues is essential to many diverse applications, such as artificial insemination, organ transplantation, virus research [1], and the preservation of endangered species [2]. However, if ice crystals form inside cells during the cooling process, this usually leads to cell death [3]. Vitrification is a cryopreservation process in which the sample is preserved in a glassy state and is one of the means by which cellular damage can be avoided [4]. Vitrification requires high concentrations of molecules that facilitate formation of the glassy state and sufficiently fast cooling rates that crystallization can be avoided [5].

In nature this is achieved by the accumulation of high concentrations of disaccharides (sucrose and trehalose), which occur in significant quantities in certain plants, seeds, and invertebrates adapted to endure desiccation and freezing [6,7]. The success of small sugars as cryoprotectants has two major facets: first, they reduce dehydration damage to cell membranes, through mechanisms that have been investigated at length [8–13]; and second, they encourage vitrification, which is the focus of this work.

In nature these molecules are created inside cells. However, they are not suitable on their own as artificial cryprotectants as they are not membrane-permeating and cannot penetrate cells. In cryopreservation, it is common to use permeating cryoprotectants such as DMSO, which can encourage vitrification and hinder ice formation, but high concentrations of such cryoprotectants are chemically toxic, disrupting membranes and damaging cells. This can be mitigated somewhat by combining glass-forming sugars with lower concentrations of permeating cryoprotectants to achieve successful cryopreservation or desiccation tolerance [14,15].

This study focusses on trehalose, which has the highest glass transition temperature of any of the disaccharides [6,9,10], though the physical mechanisms underlying this are far from clear. It is a nonreducing disaccharide that results from the combination of two D-glucopyranose molecules through $(1 \rightarrow 1)$ glycosidic linkages. The α,α-trehalose dimer is shown in Fig. 1. The propensity for solutions of trehalose to vitrify has been attributed by some workers to its ability to alter the water structure, making it less ordered and thus hindering ice formation [11–13]. It has also been suggested that the vitrification properties are closely related to its ability to affect the dynamics of the water [9,12].

In studies of the change in dynamics of the solution in the lead up to vitrification, great attention is paid to single-particle dynamics, often through study of the self-diffusion coefficient [16]. Though this property does provide useful information on the decrease in mobility in the approach to the glass transition, our previous work on colloidal suspensions [17,18] has highlighted the importance of the collective dynamics, as seen through the interdiffusion coefficients, in determining whether a system will form a glass. That work showed that the glass transition in bimodal colloidal dispersions is correlated with a decrease in a particular interdiffusion coefficient D_- to a negligible value, resulting in a plateau forming in the

*peter.daivis@rmit.edu.au

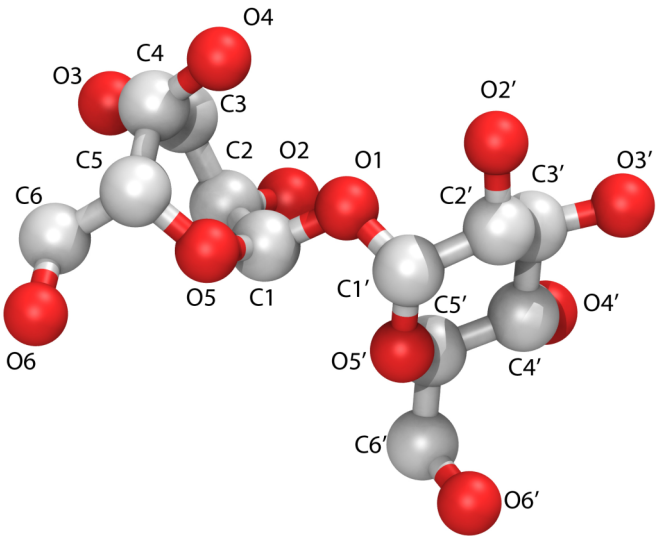

FIG. 1. α,α-Trehalose where hydrogen atoms have been omitted for clarity. All carbon and oxygen atoms have been labeled.

intermediate scattering function that signifies the formation of a glass.

This D_- coefficient is an eigenvalue of the 2×2 matrix of interdiffusion coefficients for the ternary colloidal fluid, and is directly related to the system's ability to make compositional changes. Since compositional changes are often necessary for a quenched multicomponent system to meet the local stoichiometry for crystallization, it was hypothesized that in this case, the inability to make compositional changes was the cause of the observed crystallization inhibition, which ultimately led to the formation of a long-lived metastable glassy state.

The viscosity and self-diffusion coefficient both decrease as the concentration of a binary solution increases or its temperature decreases, regardless of its glass-forming ability. In other words, the mobility of the solute decreases as the freezing point is approached via a concentration increase or a temperature decrease for both crystalizing and vitrifying solutions. However, this is not necessarily the case for the mutual diffusion coefficient, which is a product of a mobility and a thermodynamic factor. This can be seen, for example in our results for the concentration dependence of the mutual diffusion coefficient of a model unimodal (monodisperse) colloidal dispersion [17]. When polydispersity is introduced, it can have a dramatic effect. In the bimodal colloidal dispersion that we previously studied, we found that the diffusion coefficient governing changes in composition at fixed total concentration decreased dramatically to nearly zero for a glass-forming system. Strong inhibition of crystallization can also be observed in binary systems when the size ratio of the two components is in the appropriate range. In this case, the mutual diffusion coefficient is correspondingly seen to decrease as the concentration is increased [19].

There has recently been strong interest in the role of compositional changes in controlling the rate of crystallization. Nandi *et al.* [20] studied the effects of alloy composition on crystallization. They found that in some binary alloys the glass-forming ability of the alloy depended strongly on composition, and that in some cases at least, the glass-forming ability increased when the entropy penalty for demixing of the alloy in the interfacial region was maximized. Demixing is a collective process governed by both kinetic and thermodynamic factors, similar to the mutual diffusion coefficient that we study here.

Pedersen *et al.* [21] have recently found that the well-known Kobb-Andersen model of a glass-forming alloy composed of 80% large A particles and 20% smaller B particles actually crystallizes after a sufficiently long time into an FCC crystal of pure A particles in coexistence with a solution of A plus B. Again, the inhibition of crystallization is sensitive to the composition in such a way that general slowing down of the dynamics is not sufficient to explain the optimisation of the glass-forming ability of the alloy. A property such as the mutual diffusion coefficient, which incorporates both thermodynamic and frictional factors may provide useful information on the complex interplay between composition, frictional slowing, and glass-forming ability.

A phase-field modeling study of compositional relaxation dynamics for a glass-forming binary atomic mixture via the intermediate scattering function published by Berry and Grant [22] also supports the view that collective, rather than single-particle frictional properties are most relevant to models of caging and crystallization inhibition. The two models featured in their work both include a parameter that accounts for the temperature dependence of the collective mobility associated with the decay of composition fluctuations. This essentially corresponds to the inverse of the collective friction factor appearing in the mutual diffusion coefficient.

Our aim in this work is to determine whether the behavior observed in our previous study of bimodal colloidal fluids is more universal. In particular, we ask whether similar behavior can be observed in a water-saccharide solution on the approach to the glass transition. Water-saccharide solutions and colloidal suspensions are both glass-forming systems but differ greatly in the sense that the latter can be considered analogous to simple atomic or hard-sphere alloys, while the former is a solution of complex nonspherical molecules. Therefore, if such an analogous relationship exists, it may point to common underlying physical principles governing these two systems.

When ice crystals form and grow in a solution they exclude the solutes, and thus the concentration of the solutes increases in the unfrozen solution. This is known as the freeze-concentration effect [23]. One of the suggested cryopreservation mechanisms for trehalose is that, as the solute is excluded from the crystal, there is a local increase in the solute concentration near a growing ice interface, which inhibits ice-crystal growth [24]. The ability of the solution to demix and allow ice crystals to grow relies on its ability to make compositional changes at the interface.

In the saccharide solution, the transport coefficient that determines the relaxation of composition is the mutual diffusion coefficient D_m. It determines how quickly a concentration gradient (or concentration fluctuation) will decay. Though there have been some experimental measurements of D_m for other saccharide solutions [25], to the authors knowledge the data for trehalose is extremely limited [26]. Therefore, this will be one of the first studies of the mutual diffusion

coefficient of trehlose across a broad temperature and concentration range. D_m can also be related to the decay of the intermediate scattering function [27,28], which is a key quantity measured in dynamic scattering that shows the arrest of concentration fluctuations in the approach to the glass transition. If D_m plays the same role in vitrification in the saccharide solution as D_- does in the colloidal suspension, then it would offer valuable insight into the processes involved in vitrification, and may help to explain why trehalose is such a good vitrifier compared to other disaccharides.

The outline of this paper is as follows: first we give a summary of the computational model used, and describe how we calculate the mutual diffusion coefficient in equilibrium MD using time correlation functions. Then we independently determine the glass transition temperature of the solution by quenching to low temperatures, and calculate the constant pressure heat capacity upon heating. We go on to examine how the mutual diffusion coefficient (and all the factors that contribute to it) behave on the approach to the previously determined glass transition temperature.

We then perform a multiexponential analysis of the water intermediate scattering function over the same range of concentrations and temperatures, to show that the long-time decay of the intermediate scattering function is governed by the mutual diffusion coefficient. We demonstrate that the extremely long relaxation time of the fluid, which manifests as an extremely slow decay, and ultimately the arrest of the intermediate scattering function, is linked to the reduction of D_m to a negligible value. This allows a physical interpretation of the cause of the glass transition in this system, and shows a striking similarity between the underlying physics governing the mechanism of the glass transition in the saccharide solution and the colloidal suspension.

II. THEORY

A. Intermediate scattering function

The molecular intermediate scattering function $F_{\alpha\beta}(k,\tau)$ is defined as the normalized auto-correlation function of a Fourier component of the molecular number density:

$$F_{\alpha\beta}(k,\tau) = \frac{1}{N}\frac{\langle n_\alpha(\mathbf{k},\tau) n^*_\beta(\mathbf{k},0)\rangle}{S_{\alpha\beta}(k)}, \tag{1}$$

where $n_\alpha(\mathbf{k},t)$ is given as

$$n_\alpha(\mathbf{k},t) = \sum_{j=1}^{N_\alpha} \exp[-i\mathbf{k}\cdot\mathbf{r}_j(t)], \tag{2}$$

where N is the total number of molecules, N_α is the number of molecules of species α, and $\mathbf{r}_j(t)$ denotes the center of mass position of molecule of particle j at time t. The static structure factor $S_{\alpha\beta}(k)$ is defined as

$$S_{\alpha\beta}(k) = \frac{1}{N}\langle n_\alpha(\mathbf{k},0) n^*_\beta(\mathbf{k},0)\rangle, \tag{3}$$

where * signifies the complex conjugate. In an MD simulation, the wave vector $\mathbf{k}$ being studied must be consistent with the periodic boundary conditions of the simulation box:

$$\mathbf{k} = \frac{2\pi}{L}(a_1, a_2, a_3), \tag{4}$$

where a_i is an integer and L is the length of the simulation box (in this work the box is cubic so $L_x = L_y = L_z$).

From Eq. (4) we see that the lowest nonzero k value that can be studied in an MD simulation has a magnitude of $|\mathbf{k}_{\min}| = 2\pi/L$. As the fluid is isotropic the functions $F_{\alpha\beta}(k,\tau)$ and $S_{\alpha\beta}(k)$ only depend on the magnitude $k = |\mathbf{k}|$, so an average is done over all $\mathbf{k}$ of equal magnitude. The intermediate scattering functions shown in this work will all be molecular center of mass density autocorrelation function of the water molecules $F_{11}(k,\tau)$. To simplify the notation the subscripts will be dropped, and we will simply denote $F(k,\tau) = F_{11}(k,\tau)$. However, if we need to distinguish between the two species, then subscript 1 represents the water, while subscript 2 represents the trehalose.

B. Calculation of the mutual diffusion coefficient

The mutual diffusion coefficient can be calculated from equilibrium MD simulations using a combination of Green-Kubo [29,30] and Kirkwood-Buff theory [31]. The diffusion coefficient for a two-component isothermal fluid is defined by the linear flux-force relation [32]:

$$\mathbf{J}_1^0 = -D_m \nabla n_1, \tag{5}$$

where $\mathbf{J}_1^0$ is the diffusive molecular flux defined as

$$\mathbf{J}_1^0 = n_1(\mathbf{v}_1 - \mathbf{v}^0). \tag{6}$$

Here, $\mathbf{v}_1$ is the center of mass velocity of the water molecules and $\mathbf{v}^0$ is the volume average streaming velocity given by

$$\mathbf{v}^0 = \sum_{\alpha=1}^{2} n_\alpha v_\alpha \mathbf{v}_\alpha, \tag{7}$$

where v_α is the partial molecular volume of species α.

The diffusion coefficient is defined in terms of the flux measured relative to the volume average streaming velocity, but it is more convenient for computation to calculate the phenomenological coefficients defined by flux laws expressed in terms of the barycentric (mass average) streaming velocity. The relationship between the phenomenological coefficients with respect to one reference velocity and the diffusion coefficients measured relative to another can be written as [32]

$$D_m = \frac{L_{11} n_2 v_2}{c_2^2}\left(\frac{\partial \mu_1}{\partial n_1}\right)_{p,T,n_2}, \tag{8}$$

where L_{11} is the phenomenological coefficient, μ_1 is the chemical potential of the water, c_2 is the mass fraction of trehalose, and p is the pressure. Therefore, to determine the mutual diffusion coefficient we need to determine the thermodynamic factor $\partial\mu_1/\partial n_1$, the partial molecular volume of the sugar v_2 and phenomenological coefficient L_{11}.

The phenomenological coefficient is calculated from Green-Kubo theory [29,30], which states that

$$L_{11} = \frac{V}{3k_B T}\int_0^\infty \langle \mathbf{J}_1(\tau)\cdot\mathbf{J}_1(0)\rangle d\tau, \tag{9}$$

where T is the temperature, and $\mathbf{J}_1$ in this instance is calculated in the barycentric reference frame of the simulation box. The thermodynamic factor and partial volumes can be

calculated from Kirkwood-Buff theory [31]. The well-known expression found by Kirkwood and Buff states that for a fluid with two species the thermodynamic factor is calculated from

$$\frac{1}{k_B T}\left(\frac{\partial \mu_1}{\partial n_1}\right)_{p,T,n_2} = \frac{1}{n_1} + \frac{G_{12} - G_{11}}{1 + n_1(G_{11} - G_{12})}, \tag{10}$$

and the partial volume of species 2 from

$$v_2 = \frac{1 + n_1(G_{11} - G_{12})}{n_1 + n_2 + n_1 n_2(G_{11} + G_{22} - 2G_{12})}. \tag{11}$$

The volume integrals of the radial distribution functions $G_{\alpha\beta}$ are calculated from

$$G_{\alpha\beta} = \int (g_{\alpha\beta}(\mathbf{r}) - 1)\, d\mathbf{r} = 4\pi \int r^2 (g_{\alpha\beta}(r) - 1) dr, \tag{12}$$

where $g_{\alpha\beta}(r)$ is the radial distribution function of species α and β. These integrals can be difficult to calculate as statistical error in $g_{\alpha\beta}(r)$ at large r is magnified by the factor of r^2, so the numerical integrals may not converge. As was shown in the previous work [17,18], a much simpler way to calculate this quantity is through the partial structure factors:

$$G_{\alpha\beta} = \frac{1}{x_\alpha x_\beta n}\left[\lim_{k\to 0} S_{\alpha\beta}(k) - x_\alpha \delta_{\alpha\beta}\right], \tag{13}$$

where n is the total molecular number density of all species. By calculating the low-k values of the partial structure factors $S_{\alpha\beta}(k)$, and extrapolating to $k \to 0$, the values of $G_{\alpha\beta}$ can be calculated in a much simpler way.

C. Multiexponential analysis

One goal of this work is to determine the effect that trehalose has on the decay of the intermediate scattering function, to determine whether the long-time decay can be associated with the mutual diffusion coefficients. We do this via a multiexponential analysis technique similar to our previous work for the colloidal system [17,18], which is ultimately based on the arguments of Barocchi and coauthors [33]. They showed that the complete behavior of any normalized autocorrelation function of a classical many-body system can be described by a generalized Langevin equation, the exact solution of which can be written as an infinite sum of exponential functions,

$$C(t) = \sum_{j=1}^{\infty} A_j \exp(z_j t), \tag{14}$$

where A_j and z_j are mode amplitudes and decay coefficients, respectively. Such modes can be associated with relaxation channels in the system. If A_j and z_j are complex quantities, then the corresponding mode and its complex conjugate are both present in the series and, taken together, they represent an exponentially damped oscillation. Otherwise, real A_j and z_j define a purely exponential decay. An approximate solution to the generalized Langevin equation can be found by truncating Eq. (14) at a finite number of terms. The behavior of the coefficients can then be studied by fitting the resulting function to experimental and simulation data. This procedure can be difficult, due to the large number of free fitting parameters. Barocchi and coauthors found that the number of free fitting parameters can be reduced by constraining the solution. They showed that the zero time properties of the solution given in Eq. (14) must obey the relation

$$\left[\frac{d^m C(t)}{dt^m}\right]_{t=0} = 0, \tag{15}$$

where m is an odd integer. When a finite number of exponential terms are retained, Eqs. (14) and (15) can only be valid for m up to a certain value depending on the approximation level and the model assumed. The combination of Eqs. (14) and (15) allows the number of free fitting parameters to be reduced.

The minimum number of terms that need to be retained in Eq. (14) to accurately fit the intermediate scattering function data depends on the state point being studied. However, we found that for the pure water system at the wave vectors and temperatures we studied, three real and one complex mode was needed to model the complex decay of the intermediate scattering function. The addition of the trehalose molecules causes an additional real exponential decay mode to emerge which decays orders of magnitude slower than any of the decay modes observed in the pure water system. We will endeavour to show that this additional slow decay mode is associated with relaxation of composition and has a decay rate proportional to the mutual diffusion coefficient.

III. SIMULATION METHODS

In this work we have chosen to model the trehalose molecule using the OPLS potential [34], which was developed for liquid systems and has been further optimized for all-atom simulations of carbohydrate solutions [35]. It is a fully flexible, all-atom model which includes charges, Lennard-Jones (LJ) interactions, as well as linear bond length, bond angle, and dihedral potentials. The parameters for a bending interaction between an sp3 carbon-ether oxygen-acetal carbon were used to approximate the bending at the glycosidic linkage. A detailed description of the implementation of the OPLS force field is given elsewhere [36]. In this work we use the SPC/E potential [37] for the water molecules in the solution. This model is rigid and unpolarizable but still captures many of the correct properties of real water. It has been shown to reproduce the glass transition temperature better than other nonpolarizable water models [38]; however, it does not accurately reproduce details of the equilibrium phase diagram of water. Clearly, it would be best to use a model that reproduces all of these properties. However, such a model does not currently exist, so the SPC/E model is used here as it best reproduces the glass transition, which is the focus of this study.

All of the models used in this work include LJ and coulombic interactions. The trehalose molecule has bonded interactions with spring potentials, while the bonds on the water molecule are held fixed using the SHAKE algorithm. The LJ parameters were chosen from the references above [35]; the cutoff distance in this work was set to 12 Å for all atoms. The usual Lorentz-Berthelet combining rules were used to calculate cross-interaction parameters. A long-range correction was applied to the energy and virial to account for the truncation of the potential at the cutoff. The

TABLE I. Weight % concentration of trehalose, number of water molecules N_W, number of trehalose molecules N_T, and glass transition temperature found T_g.

Weight %	N_W	N_T	$T_g(K)$
0	1728	0	180
2.2	1728	2	181
9.0	1728	9	180
80.0	256	64	255
95.0	64	64	306

long-range Coulombic interactions were calculated using the Ewald summation method.

All simulations were run using the MD package LAMMPS [39] and results were post-processed using in-house code. Simulations at each packing fraction were done under NPT conditions at a range of temperatures but always at a constant pressure of 1 atmosphere. The time integration scheme used follows the time-reversible measure-preserving Verlet integrator derived by Tuckerman *et al.* [40] with a time step of 1 fs. The temperature is held fixed using a Nosé-Hoover thermostat while the pressure is held fixed using a Nosé-Hoover type barostat, both with a damping parameter of 100 fs. The number of water and trehalose molecules in each simulation is shown in Table. I.

At each concentration we attempted to study systems at temperatures close to the glass transition temperature T_g. However, the ability to do this was limited at higher concentrations as the trehalose molecules were not completely soluble at certain temperatures, resulting in a solution that was inhomogeneous. At higher trehalose concentrations, analysis of the structure factor $S(k)$ showed the solution to be inhomogeneous, possibly due to aggregation of the solute. Only results for homogeneous systems are discussed in this paper. The method for determining T_g will be shown next.

IV. RESULTS

A. Glass transition temperature

To study the dynamics on the approach to the glass transition, we must first determine the glass transition temperature for this model at each concentration. We determined the glass transition temperature by following a technique that mimics the procedure used in differential scanning calorimetry (DSC) experiments. It exploits the fact that the glass transition is indicated by an inflection in the heat capacity upon heating from a glass [38,41,42]. The procedure was as follows: Systems were equilibrated at temperatures well above the glass transition temperature (300 K for 0 wt.%, 2.2 wt.%, and 9 wt.% solutions, and 500 K for 80 wt.% and 95 wt.% solutions), then the reference temperature of the thermostat was decreased linearly in time to cool the solution. A cooling rate of 3×10^{10} K/s was used to quench the systems from the initial temperature down to 100 K. This was followed by heating back to the initial temperature at the same rate with the total enthalpy being calculated and saved every 1 ps. This was repeated 25 times and the results were averaged over all runs to improve sampling statistics. Then, we used Matlab to

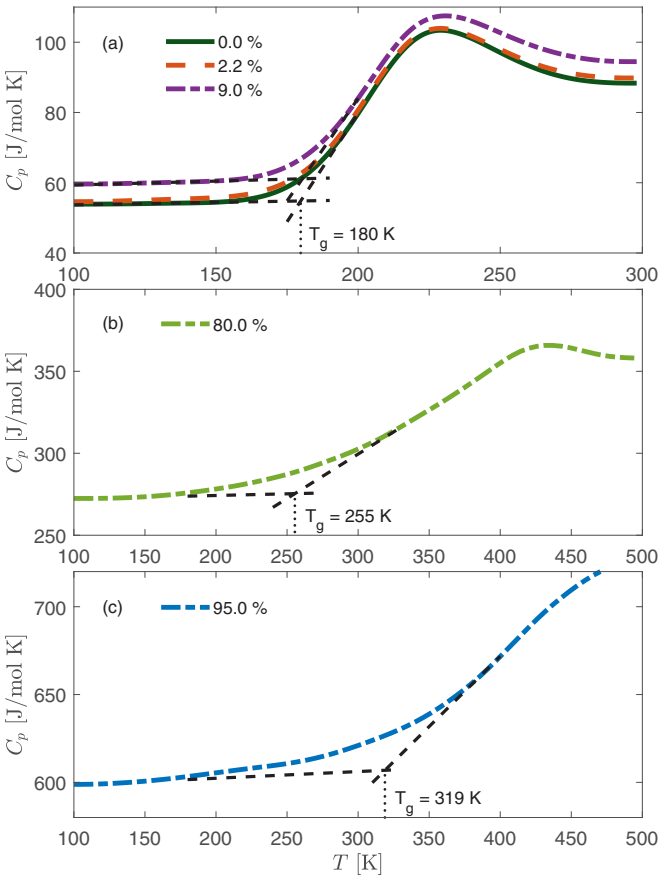

FIG. 2. Plot of the constant pressure heat capacity C_p as a function of temperature for trehalose wt.% concentrations shown in the legend.

apply a smoothing spline fit to the averaged enthalpy data with a smoothing parameter of 10^{-6} to conduct numerical differentiation. The constant pressure heat capacity C_p was calculated by numerical differentiation of the total enthalpy versus temperature. The values for C_p as a function of temperature are shown in Fig. 2 for each concentration studied. The glass transition temperature was determined by fitting the linear regions before and after the initial increase in C_p, then taking T_g as the intercept as is customary [42].

For pure water, the glass transition temperature T_g was found to be at ≈ 180 K. This is slightly lower than the value of T_g calculated by Kreck and Mancera for the same cooling rate of ≈ 188 K [38]. There is a slight arbitrariness as to which range of the data to fit which could account for the difference. Kreck and Mancera also neglected long-range corrections to the LJ potential that could also slightly shift the glass transition temperature. A value of 180–188 K is above the experimental value of T_g for pure water, which has been estimated in differential scanning calorimetry (DSC) measurements of hyperquenched water to be 136 K. This was found by detecting the small increase in the heat capacity of water associated with vitrification [43,44], though some interpret this as a prepeak preceding the true glass transition, which has been theorized to occur at the higher temperature of 165 K [43–45]. However, this cannot be tested as this falls within water's "no mans land," where crystallization occurs

too quickly for the supercooled fluid to be studied. Determining T_g from MD simulation usually results in a higher value than is found experimentally as T_g is highly dependent on the cooling rate, which is orders of magnitude faster in MD than in experiments.

The inclusion of trehalose increases the glass transition temperature, thus favoring vitrification, though not in a linear fashion. The inclusion of small concentrations of trehalose does not significantly increase the glass transition temperature. The addition of 2.2 wt.% and 9 wt.% only increases the temperature by a couple of degrees, making it difficult to resolve since the value of T_g has significant uncertainty. In line with what is observed in experiment, a large concentration of trehalose is required to raise the glass transition significantly [46].

This is observed in the higher concentration solutions shown in Figs. 2(b) and 2(c), where at 80 wt.% the glass transition temperature is estimated to be 255 K, very close to the experimental value of ≈ 252 K [46]. A further increase to 95 wt.% results in a glass transition of 311 K compared to the experimental value of ≈ 327 K [46]. Therefore, at 95 wt.% concentration the solution would now be a glass under ambient conditions. T_g is difficult to determine at higher concentration because the width of the temperature range over which the glass transition occurs was found to grow. This makes the heat capacity C_p transition less sharp, and so the extrapolation from the two linear regimes is more uncertain.

B. Mutual diffusion coefficients

To calculate accurate values for the mutual diffusion coefficient from Eq. (8), accurate values of the phenomenological coefficient L_{11}, partial molecular volume of trehalose v_2 and the thermodynamic factor $\partial\mu_1/\partial n_1$ are needed. The phenomenological coefficient L_{11} was calculated from the integral of the water molecule mass-flux correlation functions defined in Eq. (9). The mass-flux correlation functions were calculated at intervals of 5 fs out to a maximum delay time of 100 ps for the low concentrations solutions (<10 wt.%) and out to 1 ns for the high concentration solutions. This small interval of 5 fs allows for a high resolution when calculating the integral of the max flux correlation function and means any short time dynamics that may occur is captured, while the maximum delay time is chosen so that any long-time correlations have decayed away and the calculated integral will converge. Numerical integration with the trapezoid rule was performed on the correlation functions and all the integrals were found to converge within the maximum delay time. The resulting values of the phenomenological coefficients are shown in Fig. 3 for (a) 2.2 wt.% solution and (b) 95 wt.% solutions.

The L_{11} coefficient is the proportionality constant that describes how much number density flux would result from a given chemical potential gradient. As we might have expected, the value of L_{11} is observed to decrease as the temperature decreases. The lowest temperature at which this quantity was calculated at each concentration was slightly above the corresponding glass transition temperature. Attempts to calculate L_{11} at lower temperatures than T_g result in a value indistinguishable from zero, showing that the particle movement is arrested. The dependence of L_{11} on temperature is similar at

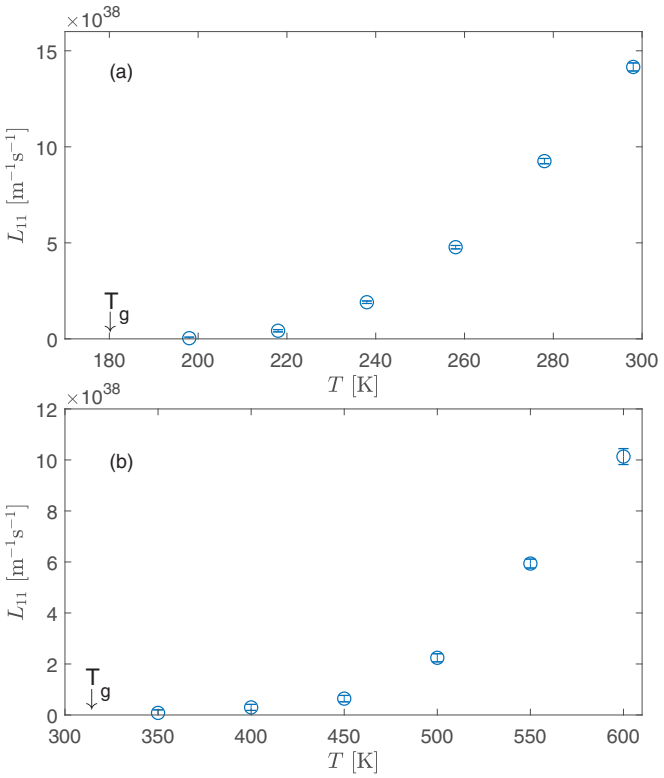

FIG. 3. Plot of the phenomenological coefficient L_{11} calculated from Eq. (9) for (a) 2.2 wt.% and (b) 95 wt.% trehalose for temperatures approaching each concentration's corresponding glass transition temperature T_g. Note the x axis scales differ.

both concentrations shown in Fig. 3. This trend is observed at all concentrations studied, though there are difficulties calculating this quantity at intermediate concentrations as the sugar is supersaturated for a larger range of temperatures above the glass transition [46]. As we will see later, it is the L_{11} coefficient that dominates the dependence of the mutual diffusion coefficients D_m on temperature for this system, rather than the thermodynamic factor or partial molecular volume.

To determine the thermodynamic factor $\partial\mu_1/\partial n_1$ and partial molecular volumes v_α, values for the integrals of the radial distribution functions $G_{\alpha\beta}$ are needed. The $G_{\alpha\beta}$ were calculated from the zero-k values of the partial static structure factors $S_{\alpha\beta}$ using Eq. (13). As an example of how the $S_{\alpha\beta}(k \to 0)$ were calculated, we have shown data for the concentration of 95 wt.% and temperature of 600K in Fig. 4. These functions are plotted against k^2 as $S_{\alpha\beta}(k)$ is found to be even in k. Although it is possible that $S(k)$ could be a nonanalytic function of k, and could therefore also depend on odd or fractional powers of $|k|$, we saw no evidence of this in our data. Therefore, to determine $S_{\alpha\beta}(k \to 0)$, a fourth-order polynomial in k^2 was fitted to S_{11} (water-water), S_{12} (water-trehalose), and S_{22} (trehalose-trehalose) data and extrapolated back to $k = 0$. At lower concentrations, a lower-order polynomial was used if it was found to fit the data well. For the low concentration systems (<10 wt.%), the S_{22} was usually quite noisy and did not have a strong dependence on k due to the small number of trehalose molecules. Therefore, to

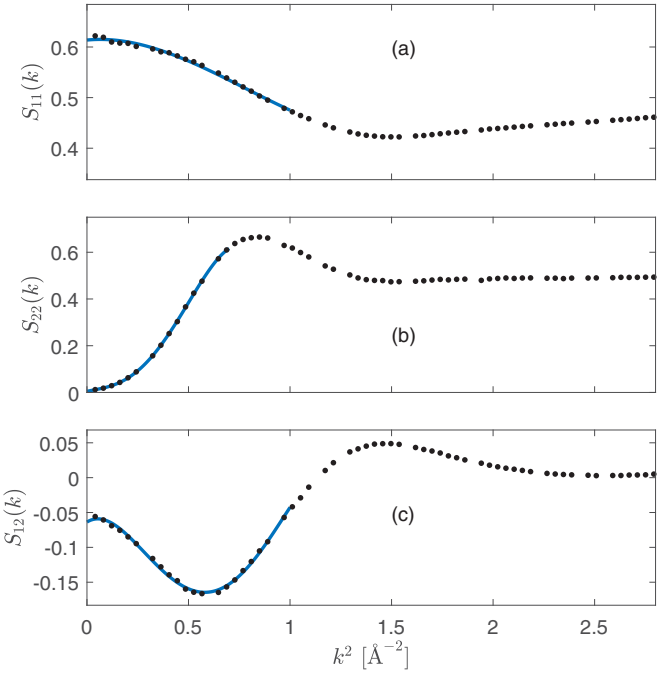

FIG. 4. Plot of the low-k values of the static structure factors of a system at a concentration of 95 wt.% and temperature of 600 K. A fourth-order polynomial line of best fit was used to obtain the $S_{\alpha\beta}(0)$ values.

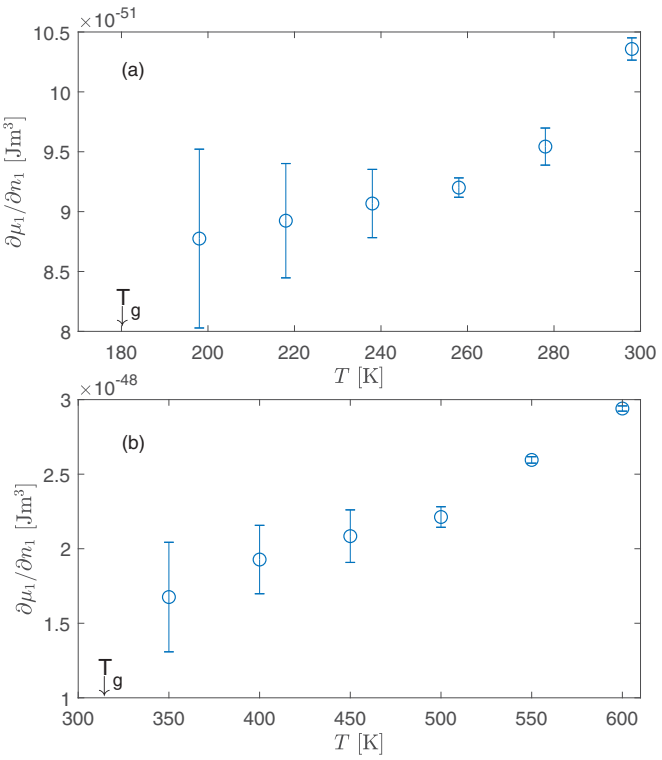

FIG. 5. Plot of the thermodynamic factor $\partial\mu_1/\partial n_1$ calculated from Eq. (10) for (a) 2.2 wt.% and (b) 95 wt.% trehalose for temperatures approaching the corresponding glass transition temperature T_g. Note the x- and y-axis scales differ.

determine $S_{22}(0)$ in these systems a simple average was taken over all the k values studied.

This analysis was done for all concentrations and temperatures studied. Then, all values calculated for $S_{\alpha\beta}(k \to 0)$ were used in Eq. (13) to calculate $G_{\alpha\beta}$. The values for $G_{\alpha\beta}$ were used in Eq. (10) to calculate the thermodynamic factor $\partial\mu_1/\partial n_1$ and Eq. (11) to calculate the partial molecular volumes v_α. The partial molecular volumes for trehalose have not been shown here, though they were found to have a qualitatively similar dependence on temperature and concentration to that seen in experimental systems [47]. The partial volume of the water molecule was found to be approximately 30 Å^3 as expected from experiment, while the trehalose molecule has a value of approximately 355 Å^3. The partial molecular volume decreases with temperature as the density of the fluid increases.

The thermodynamic factor is shown in Fig. 5 for (a) 2.2 wt.% solution and (b) 95 wt.% solution. This quantity decreases as the temperature decreases. The uncertainties also grow on the approach to T_g as it becomes more difficult to get accurate values for $S_{\alpha\beta}(k \to 0)$. The thermodynamic factor enters into the equation for the mutual diffusion coefficient [Eq. (8)] from the conversion between the true driving force of diffusion (chemical potential gradients $\nabla\mu_i$) to a quantity that can be easily measured (concentration gradients ∇n_i). It is positive as the addition of a molecule of water adds chemical potential to the solution, but its decrease in magnitude at lower temperatures is the result of individual molecules having lower chemical potential. Therefore, this quantity acts to decrease the overall mutual diffusion coefficient at lower T, but not to the same dramatic extent as L_{11}.

The mutual diffusion coefficient was calculated from Eq. (8) for all concentrations and temperatures. The mutual diffusion coefficients are shown in Fig. 6 for (a) 2.2 wt.% and (b) 95 wt.% solution, along with the glass transition temperature found for these concentrations. The mutual diffusion coefficient is observed to decrease on the approach to the glass transition temperature. The main quantities that contribute to the temperature dependence are the phenomenological coefficient L_{11} and the thermodynamic factor $\partial\mu_1/\partial n_1$, both of which decrease on the approach to the glass transition. However, it is the L_{11} coefficient decrease to zero at the glass transition temperature that causes D_m to do the same.

To the authors' knowledge this is the first time that low temperature data for the mutual diffusion coefficient of trehalose has been presented from simulation or experiment. Literature data for the mutual diffusion coefficient of trehalose even at higher temperatures is sparse at best [26], which is surprising considering that trehalose is such an important cryoprotectant molecule [48]. Therefore, we are unable to check whether the values we calculate for D_m quantitatively match with the experimental system on the approach to the glass transition temperature. There is limited experimental data available for the similar molecule sucrose that shows reasonable quantitative agreement at 298 K [25], though no data at low temperatures are available. In any case, Fig. 6 shows that D_m is observed to decrease on the approach to the glass transition at all concentrations studied, indicating that compositional relaxation slows as the temperature decreases. D_m is also observed to decrease as the concentration increases,

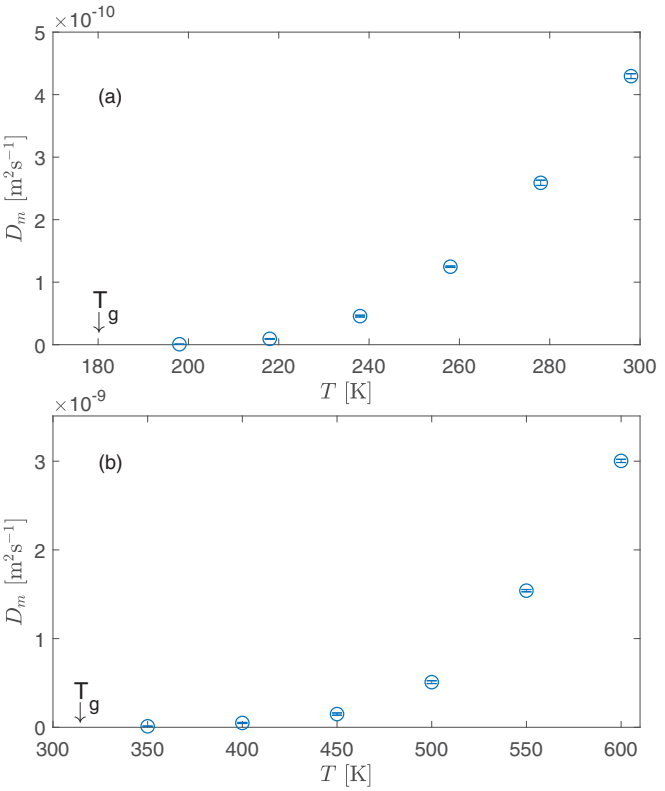

FIG. 6. Plot of the mutual diffusion coefficient D_m calculated from Eq. (8) for (a) 2.2 wt.% and (b) 95 wt.% trehalose for temperatures approaching the corresponding glass transition temperature T_g. Note the x- and y-axis scales differ.

also indicating that the addition of more trehalose molecules slows compositional relaxation. However, it is difficult to directly compare D_m at the same temperatures for different concentrations as trehalose is not completely soluble at all concentrations and temperatures.

Because of the limited accuracy with which the mutual diffusion coefficient can be calculated at low temperatures, it is difficult to determine if and where D_m extrapolates to zero. The values at the lowest temperatures measured just above T_g are found to be small but nonzero, though the trend in D_m is consistent with a decline to a negligible value at T_g, exactly as observed in the colloidal suspension [18]. This trend is observed at all concentrations studied, from the extremely low concentration shown in Fig. 6(a), to the extremely high concentrations shown in Fig. 6(b).

The decrease in D_m determines the system's ability to make compositional changes, just as the D_- coefficient was in the colloidal suspension. Therefore, the decrease in D_m to negligible values at T_g shows that the glass transition correlates with the inability of the system to make the compositional changes needed to form a stable crystal.

C. Intermediate scattering function

In this section, results for the water molecules' intermediate scattering function $F(k,\tau)$ will be shown for low concentration solutions (<10 wt.%) and extremely high concentration solutions (>80 wt.%) at temperatures approaching the glass transition temperature T_g. The wave vectors studied were those consistent with the periodic boundaries of the simulation box, given by Eq. (4) up to $a_1 = a_2 = a_3 = 10$, as our focus in this work is on the decay at low wave vectors close to the hydrodynamic limit. This is because it allows us to extrapolate to $k \to 0$ and compare the decay coefficients extracted from fits to the intermediate scattering function to the independently calculated mutual diffusion coefficients D_m.

$F(k,\tau)$ calculated for this system is shown in Fig. 7 for (a) pure water, (b) 2.2 wt.%, and (c) 9 wt.% of trehalose. A multiexponential analysis was applied to the $F(k,\tau)$ data to isolate the individual mode contributions. The number of individual decay modes that need to be retained in Eq. (14) to accurately fit the data depends on the state point and wave vector that is being studied. The data for the pure water required at most three real and one complex decay mode to accurately model the decay, owing to the complicated decay of $F(k,\tau)$ at short times. However, the addition of trehalose caused an extra long-time decay mode to appear, which we attribute to compositional relaxations.

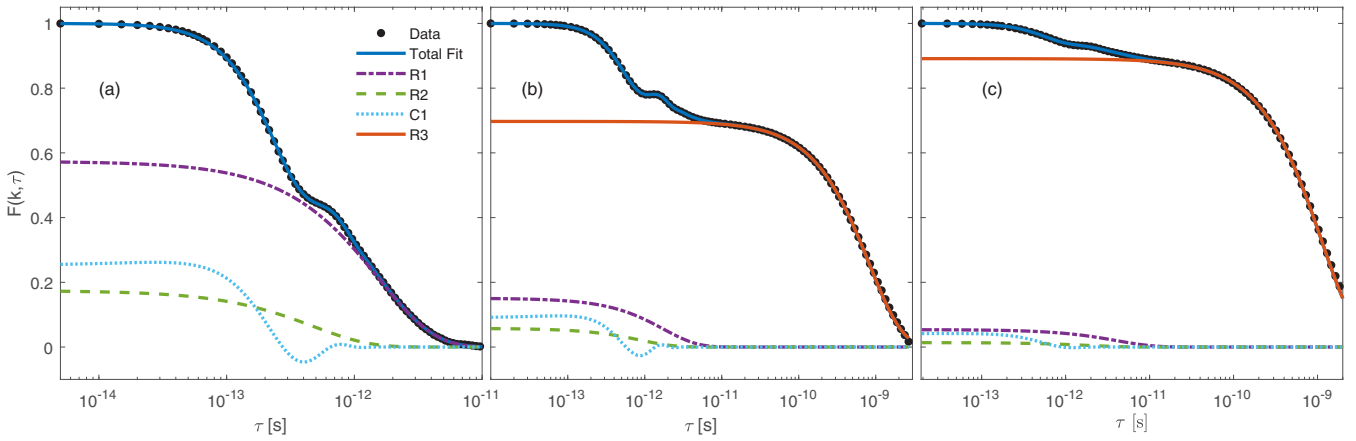

FIG. 7. Plot of the intermediate scattering function $F(k,\tau)$ of the water molecules at trehalose weight fractions of (a) 0 wt.%, (b) 2.2 wt.%, and (c) 9.0 wt.% at a low wave vector of 0.3372 Å^{-1} and temperature of 298 K. Also shown is the total multiexponential fit and the various mode contributions.

The origin of the decay modes in the pure water system shown in Fig. 7(a) is not the focus of this work, and is only calculated to set a baseline for comparison after the addition of the trehalose. For a detailed discussion of a complete method to analyze collective correlation functions for water see the work by Omelyan and coworkers [49]. However, the decaying oscillatory function that results from the complex mode in the fit (C1) could be related to the acoustic mode, and the real exponential terms (R1, R2) to the heat mode, both of which are predicted from hydrodynamic theory [50] and have been observed in pure water systems [51,52]. The focus of this work is on the additional mode that emerges when trehalose molecules are added to the solution. In Fig. 7(b) we see that at the extremely low concentration of 2.2% the original short-time modes observed in pure water are still present, however their contribution to the complete decay of the intermediate scattering function has greatly diminished. These short-time modes now only make up $\approx 40\%$ of the complete decay at 2.2 wt.%, and only $\approx 10\%$ of the decay at 9 wt.%, with this trend continuing at higher concentrations. At moderate concentrations the decay is dominated by the new long-time relaxation mode that is not present in the pure water system. This shows that the intermediate scattering function in the sugar solution does not decay via short-time dynamics, but via a different long-time mechanism.

At just 2.2 wt.%, this new mode extends the relaxation of the intermediate scattering function out by over two orders of magnitude, showing a significant slow-down in the relaxation of the Fourier components of the water molecule number density. This would have the effect of inhibiting the crystallization of the water as the compositional changes needed to meet the stoichiometry of a crystal containing trehalose and water would occur very slowly. This crystallization inhibition is observed experimentally through the large effect that the solute has on lowering the homogenous nucleation temperature T_h of the water, which is the lowest temperature that supercooled water can achieve using experimental cooling rates before crystallization occurs. However, it is interesting to note that even though the dynamics of the water molecules has slowed down, it is not enough to noticeably raise the glass transition temperature at these cooling rates. As we saw in Fig. 2, large concentrations of trehalose are needed to increase the relaxation time by enough to result in a significant increase in T_g at these ultra fast cooling rates.

It has been shown in ionic liquids [27], liquids containing dissolved gases [53,54], binary Lennard-Jones fluids [28] and model colloidal suspensions [17,18] that the slowest decay mode observed in the intermediate scattering function is related to interdiffusion coefficients. It is conceivable that the slowest decay mode in this sugar solution may be a different process that is not related to collective diffusion, so here we seek to determine the source of the long-time mode in the intermediate scattering function. To do this we extracted the decay-coefficients of the long-time mode from the fits to compare against the independently calculated D_m values given in Fig. 6(a). The extracted decay coefficients are shown in Fig. 8(a) (symbols) along with the independently calculated mutual diffusion coefficients (arrows).

The decay coefficient seems to be wave-vector-independent, so to determine the $k \to 0$ value an average was done over the wave-vector range shown, and is indicated by the dashed line in Fig. 8(a). As can be observed, in the $k \to 0$ limit the decay coefficients of the long-time decay of the intermediate scattering function are in good agreement with the independently measured mutual diffusion coefficients, as was found in the colloidal system [18]. This can be shown at all concentrations provided that the long-time exponential decay mode can be isolated. This becomes harder at higher concentrations or lower temperatures, as the maximum wave vector needed to achieve the macroscopic diffusive limit (where we see exponential decay) decreases, so larger simulation sizes are needed (since $k_{\min} = 2\pi/L$). This is evidence that the slowest collective process limiting the decay of the intermediate scattering function is also compositional relaxation.

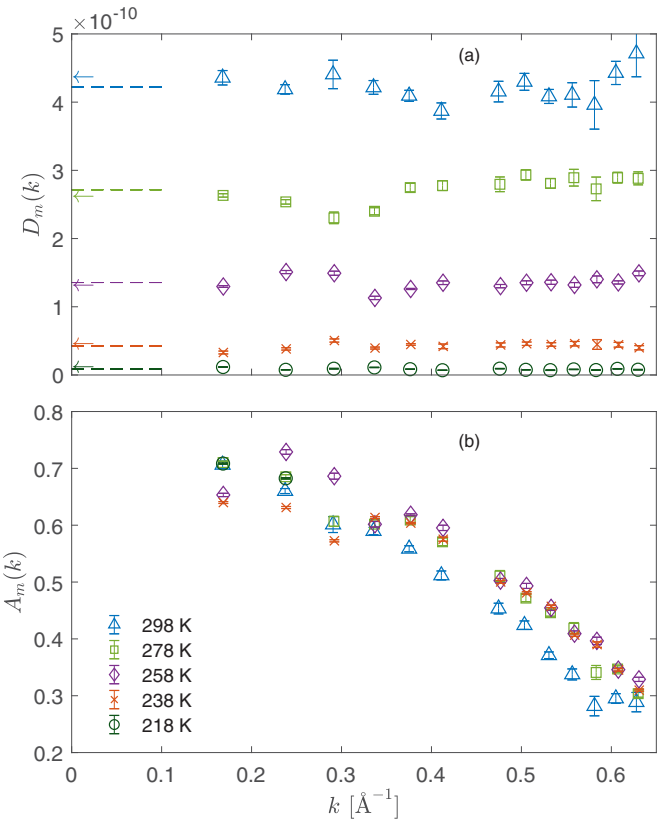

FIG. 8. Plot of wave-vector-dependence of the long-time mode (a) decay coefficients $D_m(k)$ and (b) amplitudes $A_m(k)$. Data at trehalose concentration of 2.2 wt.% and temperatures shown in the legend. Independently calculated values of D_m from Fig. 6(a) are shown as arrows and dotted line shows average of $D_m(k)$ taken over the k range shown.

The amplitudes $A_m(k)$ were also extracted from the fits to the long-time mode and they are shown in Fig. 8(b). The compositional mode amplitudes have a maximum in the $k \to 0$ limit that corresponds to long wavelength density fluctuations. As k increases, shorter wavelength density fluctuations are being probed, so the compositional relaxation mode has a smaller contribution. At moderate wave vectors of $k > 0.7 - 0.8$ Å^{-1}, the amplitude of this mode decreases to where it makes an insignificant contribution to the decay of the intermediate scattering function. This type of behavior

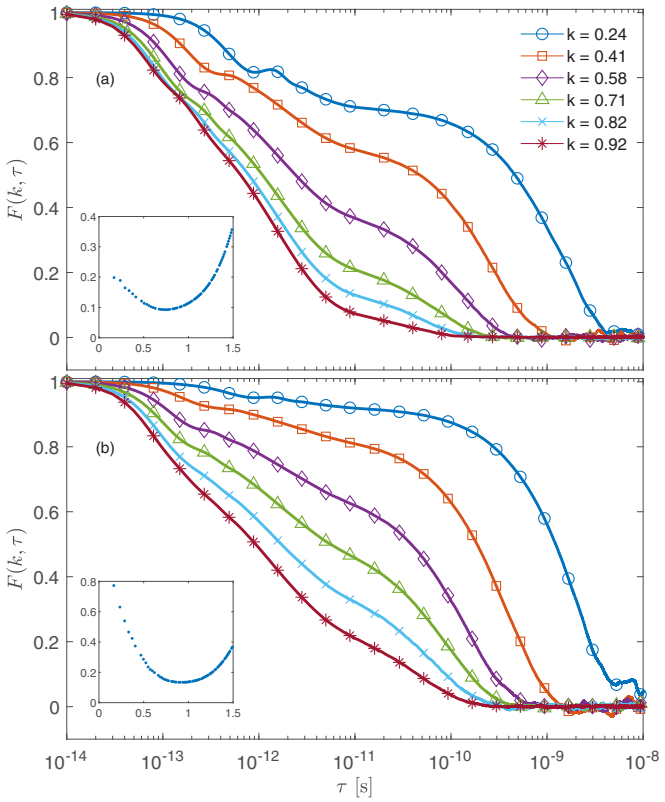

FIG. 9. Plot of the water intermediate scattering function $F(k,\tau)$ at trehalose weight fractions of (a) 2.2 wt.% and (b) 9 wt.% at 298 K for wave vectors k shown in the legend. Inset shows $S(k)$ at low wave vectors to help visualize the position of the wave vectors in the structure factor.

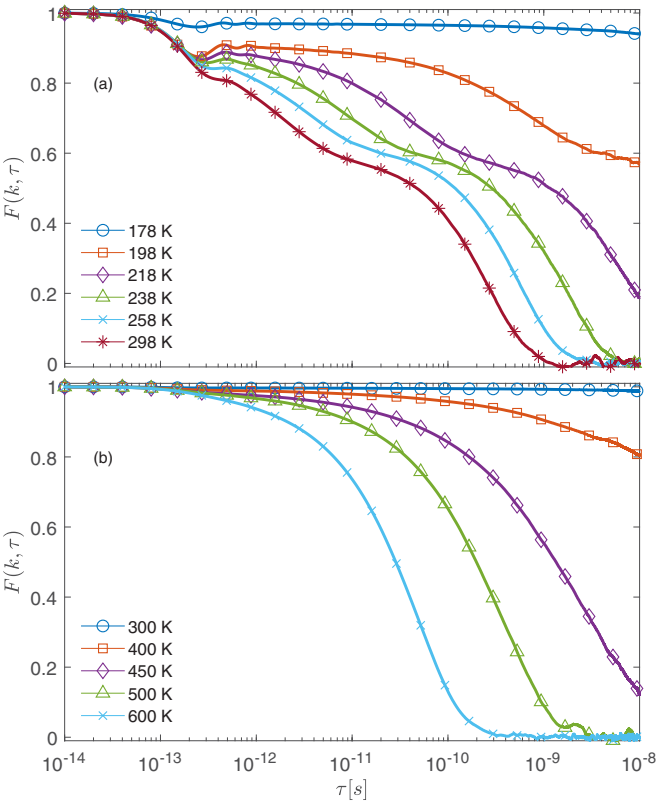

FIG. 10. Plot of the water intermediate scattering function $F(k,\tau)$ at trehalose weight fractions of (a) 2.2 wt.% and (b) 95.0 wt.% at $k = 0.33$ Å^{-1} for temperatures leading down to the glass transition.

was also observed in the colloidal suspension [18] and we explained this by saying that high-k density fluctuations would decay via small-scale local movements, and would not need large scale compositional rearrangements to decay.

To better visualize the wave-vector-dependence of the compositional relaxation mode we have plotted the intermediate scattering function in Fig. 9 at a number of low wave vectors for (a) 2.2 wt.% and (b) 9.0 wt.% trehalose. The insets show the values of the structure factor $S(k)$ to help us visualize the wave vectors being probed. The decay rate of $F(k,\tau)$ is slowest at the lowest k where long wavelength density fluctuations are being probed, and it increases with increasing k as shorter wavelength density fluctuations decay faster. As we saw previously, the k dependence of $D_m(k)$ is (roughly) independent of wave vector, so the decay rate of $F(k,\tau)$ scales with k^2 as expected. This mode can be seen by the secondary hump in the decay, and we see that its amplitude is maximum in the low-k limit, and decreases as k increases. At $k \approx 1.0$ Å^{-1} the mode amplitude is quite small, showing that this process is only significant for the decay of large wavelength density fluctuations. However, as the concentration of trehalose increases, this mode persists to larger k. This can be seen be comparing the decay at $k = 0.92$ Å^{-1} at both concentrations where the amplitude is larger for the 9 wt.% solution.

Since the long-time decay of the intermediate scattering function is governed by the mutual diffusion coefficient, and this coefficient decreases on the approach to the glass transition, we expect the long-time decay of the intermediate scattering function to slow down on the approach to T_g and eventually plateau at T_g as $D_m \to 0$. Fig. 10 shows the decay of the intermediate scattering function for (a) 2.2 wt.% and (b) 95 wt.% at temperatures down to and just beyond T_g at a wave vector of 0.33 Å^{-1}. We have chosen to focus on these two concentrations as they allow us to show the two extremes in the behavior of the intermediate scattering function. Solutions at these concentrations remain single-phase at temperatures close to their glass transition temperatures, allowing us to obtain data at each state point. We note that no aging was observed for systems with temperatures above T_g.

The $F(k,\tau)$ decay at 2.2 wt.% shown in Fig. 10(a) highlights two key processes as the temperature decreases. First, the acoustic mode seen by the reversal in $F(k,\tau)$ at $\approx 4 \times 10^{-13}$ s is decaying slower as the solution becomes more solid like and the soundwave is able to propagate further as it is not being dissipated in the solution. Second, the long-time compositional mode decay, which is the limiting factor in the decay of the intermediate scattering function, decays more slowly. At temperatures below the glass transition temperature, both the sound mode and the mutual diffusion mode no longer decay on a reasonable timescale, and so we see the classic

plateau in the intermediate scattering function which signifies that a glass has formed.

The decay at 95.0 wt.% is simpler. It shows a continuation of the trend already observed in Fig. 7 at low concentrations. The addition of trehalose suppresses the short time dynamic relaxation so that the intermediate scattering function decays completely via long-time compositional relaxation. The decay rate of this mode decreases as the temperature decreases, until the relaxation time increases to well beyond the maximum delay time of the correlation function, and the system has formed a glass. At both concentrations the long-time decay rate decreases on the approach to the glass transition temperature. This results in an extremely slow decay at temperatures slightly below T_g. This shows that over the timescale observable in our MD simulations, the slowing down and eventual "arrest" that is observed in the long-time tail of the intermediate scattering function is directly linked to the slow-down and arrest in compositional relaxations.

V. CONCLUSION

Molecular dynamics simulations were conducted on a model trehalose solution to study its behavior on its approach to the glass transition. In this study, we sought to determine whether the arrest of compositional relaxations could be linked to the glass transition of the solution, a link which has been observed in model colloidal suspensions. We first determined the glass transition temperature of the solution at various concentrations by quenching the fluid and calculating the constant pressure heat capacity. A sudden inflection in the heat capacity allowed us to determine T_g. We found that small concentrations of trehalose ($<$9 wt.%) did not increase T_g by a measurable amount, but very large concentrations $>$80 wt.% had a large effect on T_g.

The mutual diffusion coefficients were calculated from equilibrium MD simulations using a combination of Green-Kubo and Kirkwood-Buff theory. This was done for a number of temperatures and concentrations, which is the first time that the mutual diffusion coefficient (and all the factors that contribute) has been determined for concentrated trehalose solutions in simulation or experiment. D_m was found to decrease with increased trehalose concentration. It also decreased with temperature showing that composition is relaxing more slowly at lower temperatures. This culminated in a decrease to negligible values at T_g, something that has also been observed in colloidal suspensions. This demonstrates that these two very different glass-forming systems have something in common: Under conditions where the composition cannot relax, they are not able to reach their equilibrium structure within the simulation time window.

The mutual diffusion coefficient was shown to correspond to the slowest decay mode in the intermediate scattering function at low wave vectors. Therefore, the decrease in D_m to negligible values resulted in an extremely slow decay in the intermediate scattering function and the formation of a plateau, which is usually associated with the arrest and glass formation. This slow decay mode was found to become more dominant as the concentration increases, showing that the relaxation of the intermediate scattering function at large concentrations is dominated by the relaxation of composition.

This work shows the importance of the mutual diffusion coefficient and the relaxation of composition to the process of vitrification. While the self-diffusion coefficient and the viscosity both decrease as solidification is approached for both good and poor glass-forming solutions, this is not necessarily the case for the mutual diffusion coefficient, which can increase with concentration for some binary solutions as they approach solidification. By observing the strong decrease in the mutual diffusion coefficient as the glass transition is approached in two very different good glass formers (polydisperse colloidal suspensions and trehalose solutions) we have identified behavior that contrasts with the increase in the mutual diffusion coefficient seen previously in a crystallizing fluid (the monodisperse colloidal suspension). This suggests that the mutual diffusion coefficient, which is far less commonly studied than the self-diffusion coefficient or the viscosity, may be useful in discriminating between good and poor glass formers. We believe it would be prudent to obtain more experimental and simulation data on the mutual diffusion coefficient in trehalose solutions as this is currently lacking. More experimental and simulation studies looking at this relationship in other glass-forming systems would also be beneficial to test the generality of the observations made.

ACKNOWLEDGMENTS

Computational resources were provided by the National Computational Infrastructure (NCI), which is supported by the Australian Government. S.D.W.H. acknowledges the Australian government for supporting this work through an Australian post-graduate award (APA). G.B. acknowledges the support of the Australian Government through the Australian Research Council Linkage Projects funding scheme (Projects No. LP140100993 and No. LP160101496).

[1] Z. Hubálek, Cryobiology **46**, 205 (2003).

[2] A. Kaczmarczyk, B. Funnekotter, S. R. Turner, E. Bunn, G. Bryant, T. E. Hunt, and R. L. Mancera, CryoLetters **34**, 508 (2013).

[3] G. Bryant, Cryobiology **32**, 114 (1995).

[4] J. Wolfe and G. Bryant, Cryobiology **39**, 103 (1999).

[5] V. Berejnov, N. S. Husseini, O. A. Alsaied, and R. E. Thorne, J. Appl. Crystallogr. **39**, 244 (2006); S. N. Bhat, A. Sharma, and S. V. Bhat, Phys. Rev. Lett. **95**, 235702 (2005); P. Brüggeller and E. Mayer, Nature **288**, 569 (1980); G. M. Fahy, B. Wowk, J. Wu, and S. Paynter, Cryobiology **48**, 22 (2004).

[6] L. M. Crowe, D. S. Reid, and J. H. Crowe, Biophys. J. **71**, 2087 (1996).

[7] J. H. Crowe, J. F. Carpenter, and L. M. Crowe, Annu. Rev. Physiol. **60**, 73 (1998); K. L. Koster and A. C. Leopold, Plant Physiol. **88**, 829 (1988); K. L. Koster, *ibid.* **96**, 302 (1991).

[8] J. H. Crowe, L. M. Crowe, A. E. Oliver, N. Tsvetkova, W. Wolkers, and F. Tablin, Cryobiology **43**, 89 (2001); G. Bryant, K. L. Koster, and J. Wolfe, Seed Sci. Res. **11**, 17 (2001);

P. Westh, Phys. Chem. Chem. Phys. **10**, 4110 (2008); H. D. Andersen, C. Wang, L. Arleth, G. H. Peters, and P. Westh, Proc. Natl. Acad. Sci. **108**, 1874 (2011).
[9] B. Kent, T. Hauß, B. Demé, V. Cristiglio, T. Darwish, T. Hunt, G. Bryant, and C. J. Garvey, Langmuir **31**, 9134 (2015).
[10] B. Kent, T. Hunt, T. A. Darwish, T. Hauß, C. J. Garvey, and G. Bryant, J. R. Soc., Interface **11**, 20140069 (2014).
[11] T. Lenné, C. J. Garvey, K. L. Koster, and G. Bryant, J. Phys. Chem. B **113**, 2486 (2009).
[12] K. L. Koster, K. J. Maddocks, and G. Bryant, Eur. Biophys. J. Biophys. Lett. **32**, 96 (2003).
[13] K. L. Koster, Y. P. Lei, M. Anderson, S. Martin, and G. Bryant, Biophys. J. **78**, 1932 (2000).
[14] G. M. Fahy, B. Wowk, J. Wu, J. Phan, C. Rasch, A. Chang, and E. Zendejas, Cryobiology **48**, 157 (2004).
[15] F. Sussich, R. Urbani, F. Princivalle, and A. Cesàro, J. Am. Chem. Soc. **120**, 7893 (1998).
[16] P. B. Conrad and J. J. de Pablo, J. Phys. Chem. A **103**, 4049 (1999); L. Weng and G. D. Elliott, Phys. Chem. Chem. Phys. **16**, 11555 (2014); N. Ekdawi-Sever, J. J. de Pablo, E. Feick, and E. von Meerwall, J. Phys. Chem. A **107**, 936 (2003).
[17] S. D. W. Hannam, P. J. Daivis, and G. Bryant, Phys. Rev. E **94**, 012619 (2016).
[18] S. D. W. Hannam, P. J. Daivis, and G. Bryant, Phys. Rev. E **96**, 022609 (2017).
[19] B. Bernu, Y. Hiwatari, and J. P. Hansen, J. Phys. C: Solid State Phys. **18**, L371 (1985).
[20] U. K. Nandi, A. Banerjee, S. Chakrabarty, and S. M. Bhattacharyya, J. Chem. Phys. **145**, 034503 (2016).
[21] U. R. Pedersen, T. B. Schrøder, and J. C. Dyre, Phys. Rev. Lett. **120**, 165501 (2018).
[22] J. Berry and M. Grant, Phys. Rev. E **89**, 062303 (2014).
[23] P. Mazur, Amer. J. Physiol. **247**, C125 (1984).
[24] T. Sei, T. Gonda, and Y. Arima, J. Cryst. Growth **240**, 218 (2002); T. Gonda and T. Sei, Prog. Cryst. Growth Charact. Mater. **51**, 70 (2005).
[25] A. C. Ribeiro, O. Ortona, S. M. Simões, C. I. Santos, P. M. Prazeres, A. J. Valente, V. M. Lobo, and H. D. Burrows, J. Chem. Eng. Data **51**, 1836 (2006).
[26] X. He, A. Fowler, and M. Toner, J. Appl. Phys. **100**, 074702 (2006).
[27] M. H. Rausch, J. Lehmann, A. Leipertz, and A. P. Fröba, Phys. Chem. Chem. Phys. **13**, 9525 (2011).
[28] J. W. Nichols and D. R. Wheeler, Ind. Eng. Chem. Res. **54**, 12156 (2015).
[29] M. S. Green, J. Chem. Phys. **22**, 398 (1954).
[30] R. Kubo, J. Phys. Soc. Jpn. **12**, 570 (1957).
[31] J. G. Kirkwood and F. P. Buff, J. Chem. Phys. **19**, 774 (1951).
[32] S. R. de Groot and P. Mazur, *Nonequilibrium Thermodynamics* (Dover Publications, New York, 1984).
[33] F. Barocchi, U. Bafile, and M. Sampoli, Phys. Rev. E **85**, 022102 (2012).
[34] W. L. Jorgensen, J. D. Madura, and C. J. Swenson, J. Am. Chem. Soc. **106**, 6638 (1984).
[35] W. Damm, A. Frontera, J. Tirado-Rives, and W. L. Jorgensen, J. Comput. Chem. **18**, 1955 (1997).
[36] W. L. Jorgensen, D. S. Maxwell, and J. Tirado-Rives, J. Am. Chem. Soc. **118**, 11225 (1996).
[37] H. J. C. Berendsen, J. R. Grigera, and T. P. Straatsma, J. Phys. Chem. **91**, 6269 (1987).
[38] C. A. Kreck and R. L. Mancera, J. Phys. Chem. B **118**, 1867 (2014).
[39] S. Plimpton, J. Comput. Phys. **117**, 1 (1995).
[40] M. E. Tuckerman, J. Alejandre, R. López-Rendón, A. L. Jochim, and G. J. Martyna, J. Phys. A: Math. Gen. **39**, 5629 (2006).
[41] C. A. Angell, Chem. Rev. **102**, 2627 (2002).
[42] C. A. Angell and S. Borick, J. Non-Cryst. Solids **307–310**, 393 (2002).
[43] A. Hallbrucker, E. Mayer, and G. P. Johari, J. Phys. Chem. **93**, 4986 (1989).
[44] V. Velikov, S. Borick, and A. C. Angell, Science **294**, 2335 (2001).
[45] Y. Yue and C. A. Angell, Nature **427**, 717 (2004).
[46] T. Chen, A. Fowler, and M. Toner, Cryobiology **40**, 277 (2000).
[47] C. Branca, S. Magazù, G. Maisano, and P. Migliardo, J. Biol. Phys. **26**, 295 (2000).
[48] H. Huang, G. Zhao, Y. Zhang, J. Xu, T. L. Toth, and X. He, ACS Biomater. Sci. Eng. **3**, 1758 (2017).
[49] I. P. Omelyan, I. M. Mryglod, and M. V. Tokarchuk, Condens. Matter Phys. **8**, 25 (2005).
[50] J. P. Boon and S. Yip, *Molecular Hydrodynamics* (Dover Publications, New York, 2013).
[51] T. Komatsu, N. Yoshii, S. Miura, and S. Okazaki, Fluid Phase Equilib. **226**, 345 (2004).
[52] C. Y. Liao, S. H. Chen, and F. Sette, Phys. Rev. E **61**, 1518 (2000).
[53] A. Heller, T. M. Koller, M. H. Rausch, M. S. H. Fleys, A. N. R. Bos, G. P. van der Laan, Z. A. Makrodimitri, I. G. Economou, and A. P. Fröba, J. Phys. Chem. B **118**, 3981 (2014).
[54] A. Heller, C. Giraudet, Z. A. Makrodimitri, M. S. Fleys, J. Chen, G. P. Van Der Laan, I. G. Economou, M. H. Rausch, and A. P. Fröba, J. Phys. Chem. B **120**, 10808 (2016).